A molecular dynamics study of heat transfer over an ultra-thin liquid film with surfactant between solid surfaces

doi: 10.1063/1.5123583

Journal of Applied Physics

A molecular dynamics study of heat transfer over an ultra-thin liquid film with surfactant between solid surfaces

Cite as: J. Appl. Phys. **126**, 185302 (2019); https://doi.org/10.1063/1.5123583
Submitted: 07 August 2019 . Accepted: 27 October 2019 . Published Online: 11 November 2019

Yuting Guo, Donatas Surblys, Yoshiaki Kawagoe, Hiroki Matsubara, and Taku Ohara

Journal of Applied Physics ARTICLE scitation.org/journal/jap

A molecular dynamics study of heat transfer over an ultra-thin liquid film with surfactant between solid surfaces

Cite as: J. Appl. Phys. **126**, 185302 (2019); doi: 10.1063/1.5123583
Submitted: 7 August 2019 · Accepted: 27 October 2019 ·
Published Online: 11 November 2019

Yuting Guo,[1,2,a)] Donatas Surblys,[2] Yoshiaki Kawagoe,[2] Hiroki Matsubara,[2] and Taku Ohara[2]

AFFILIATIONS

[1]Graduate School of Engineering, Tohoku University, Sendai 980-8577, Japan
[2]Institute of Fluid Science, Tohoku University, Sendai 980-8577, Japan

[a)]**Electronic mail:** guoyuting@dc.tohoku.ac.jp.

ABSTRACT

Using molecular dynamics simulation, we investigated the mechanism by which the intercalation of a surfactant solution reduces the contact thermal resistance of two solid surfaces. We constructed a model system where two solid surfaces with a gap were immersed in a surfactant solution, and the gap was filled with permeating molecules to form a molecular thin film. By varying the concentration of the surfactant and the distance between the confining surfaces, factors affecting the intersolid heat transfer were explored. It was demonstrated that the overall thermal resistance of the present system was determined by interfacial thermal resistance between the solid and the solution and can be reduced by increasing the surfactant concentration. The surface separation, i.e., the distance between the two solid surfaces, had a significant impact on interfacial thermal resistance, whether or not surfactant molecules were involved. Interfacial thermal resistance was an oscillatory function of the surface separation and displayed minimum values not at the most adsorption amount of liquid molecules but when the density profile of liquid molecules showed a sharp peak, i.e., when the surface separation was commensurable with the size of the solvent molecule. This tendency was most remarkably seen when the liquid film was composed of a single molecular layer. The findings in this study provide helpful insights into the reduction of interfacial thermal resistance utilizing surfactant solutions.

I. INTRODUCTION

Thermal interface material (TIM), usually as either a soft material or a liquid state, is widely used to enhance heat transfer between solid substrates by filling the joint voids.[1–3] In such cases, instead of the original thermal resistance of ambient gas in the gaps between solid surfaces, the overall thermal resistance between the solids is composed of thermal resistance in the TIM and the solid-TIM interfacial thermal resistance. In the case of nanoscale devices, where the TIM becomes thin, the interfacial thermal resistance governs the overall thermal resistance, and, therefore, surface modification is expected to be a promising way to improve the interfacial thermal conduction. Some theoretical studies attaching a nanomolecular monolayer to the solid-TIM interface in such directions have been carried out, where they found that using a strong bonding monolayer at the interface enhances the interfacial thermal conductance (ITC).[4,5]

Another way to reduce interfacial thermal resistance is the application of the surfactant, which has been widely used to facilitate the adsorption of liquid on solid surfaces.[6–9] Recent research showed that the surfactant is also applicable to improve the solid-liquid interfacial heat transfer.[10] In our previous study, we performed the molecular dynamics (MD) simulation of the surfactant solution in contact with a solid surface and demonstrated that an enhanced solid-liquid affinity by the surfactant reduces the solid-liquid interfacial thermal resistance.[11] In that study, we assumed a relatively large thickness of TIM compared with the size of the solvent or surfactant molecules and dealt with a single liquid-solid interface.

In the actual application of TIM, due to surface roughness, the distance between two contacting solid surfaces differs depending on the local position in the surface. It is, therefore, probable that at some local positions, TIM takes the form of an extremely thin

liquid film. Liquid molecules in such a film with a thickness of a few molecules are under the influence of both solid surfaces simultaneously. Some studies, including our previous work, indicated that the system of a molecularly thin liquid film confined between solid surfaces can show greatly heightened intersolid thermal conductivity,[12,13] and overall thermal resistance becomes extremely low when the film is a single layer.[13,14] For thin confined films of the surfactant solution, the concentration of the surfactant at the solid-liquid interface[15] and the micelle shape of the surfactant adsorption layer[16,17] was investigated as a function of surface separation in previous works. However, to the best of the authors' knowledge, there is little research focusing on the heat transfer over such systems.

In this study, we performed molecular dynamics simulation of systems in which two solid walls with a gap between them were immersed in a liquid TIM, and the gap was filled with the liquid TIM, where the heat conduction between solid walls under a variety of surface separations and surfactant concentrations, i.e., different states of intercalation, was investigated. Amphiphilic organic compounds are commonly used as surfactants. Such a surfactant usually contains two different functional groups, where each group has high affinity to either the solid or solvent, respectively.[7,10,18] However, having two functional groups is not always necessary for a molecule to serve as a surfactant; the amphipathicity to the solid and solvent can also be achieved via other approaches. To explore the fundamental molecular mechanism of surfactant adsorption affecting the interfacial heat transfer, the surfactant and the solvent are simplified to monatomic molecules, and the strengths of molecular interactions are chosen so that the affinity of surfactant-solvent and that of surfactant-solid are higher than that of solvent-solid. With this setting, our system reasonably realizes the properties of a solvent-surfactant-solid system. The molecular mechanism of heat conduction was analyzed by decomposing interfacial thermal conductance (ITC) into the contributions from microscopic heat transfer between different atomic species.

Details of our simulation are given in Sec. II. The adsorption structures of the solution are illustrated in Sec. III A, and the response of the thermal resistance to the surface separation is given in Sec. III B The interface concentration, adsorption amount, and liquid molecular alignment at various conditions are discussed in Sec. III C. Analysis of vibrational density of states (VDOS) is provided in Sec. III D. The decomposition of interfacial thermal conductance and its correlation with the solid-liquid affinity is discussed in Sec. III E.

II. SIMULATION DETAILS

The present study requires MD simulations for a system of solid walls and a liquid. The liquid is composed of a solvent and a surfactant. The interaction between liquid molecules (surfactant-solvent, surfactant-surfactant, solvent-solvent) was given by the Lennard-Jones (LJ) potential

$$\phi(r_{ij}) = 4\varepsilon\left[\left(\frac{\sigma_{ij}}{r_{ij}}\right)^{12} - \left(\frac{\sigma_{ij}}{r_{ij}}\right)^{6}\right], \quad (1)$$

where the parameters for argon[19] were applied for surfactant-solvent, surfactant-surfactant, solvent-solvent interactions: $\sigma = 3.4236$ Å and $\varepsilon = 1.65 \times 10^{-21}$ J.

TABLE I. Interaction parameters between different molecular types obtained from Fig. 3(b) of Ref. 21.

Interaction species	ε ($\times 10^{-21}$ J)
Solvent-surfactant	1.65
Solvent-solvent	
Surfactant-surfactant	
Solid−surfactant	1.25
Solid−solvent	0.66

Platinum was assumed for the solid walls, and the interaction between solid molecules was modeled by the Morse potential

$$\phi(r_{ij}) = D\left[e^{-2\alpha(r_{ij}-r_0)} - 2e^{-\alpha(r_{ij}-r_0)}\right], \quad (2)$$

where the parameters were taken from Ref. 20 as $D = 1.16214 \times 10^{-19}$ J, $r_0 = 2.91049$ Å, and $\alpha = 1.62597$ Å^{-1}.

The solid-liquid interaction was also expressed by the LJ potential, where the surfactant and solvent molecules were distinguished by varying the potential well depth value ε of the solid-liquid interaction as listed in Table I. In order to achieve amphiphilicity in our monoatomic system, potential well depths were set to give a contact angle of 0° and 90° for the surfactant and the solvent on an FCC (111) surface, respectively,[21] i.e., the affinity of solid-surfactant is higher than that of solid-solvent. As mentioned previously, the surfactant-solvent interaction was treated the same as solvent-solvent, and hence, the surfactant molecules also have a high affinity with solvent molecules. The solid-liquid radius parameter was set as 2.935 Å for both the solid-surfactant and solid-solvent.[21] A potential cutoff radius of 3.5σ and a time step of 1 fs were used for all simulations with the velocity Verlet integrator. The atomic mass of the liquid (the surfactant and solvent) was set to the mass of argon atom: 6.63×10^{-26} kg, and the solid was set to that of platinum atom: 3.23×10^{-25} kg.

In the present study, the schemes of MD simulations were composed of two phases. In the first phase, the liquid structure of a thin film under a constant temperature gradient was obtained from a large system where the pressure and bulk concentration of the surfactant were controlled. In the second phase, we recreated a small system with the same condition as the first phase and carried out the data analysis.

A. First phase

In the first phase, using LAMMPS MD package,[22] we randomly placed 22 000 liquid molecules in a large system as shown in Fig. 1(a), where two solid walls were prepositioned. The liquid was composed of a surfactant and solvent molecules with a variety of concentrations as a simulation parameter. The middle layer of each solid wall was fixed to keep the solid walls in place during the simulation. Three-dimensional periodic boundary conditions were applied to the system. The x-dimension and initial y-dimension of the system were 5.5 nm and 31.2 nm, respectively, while two solid

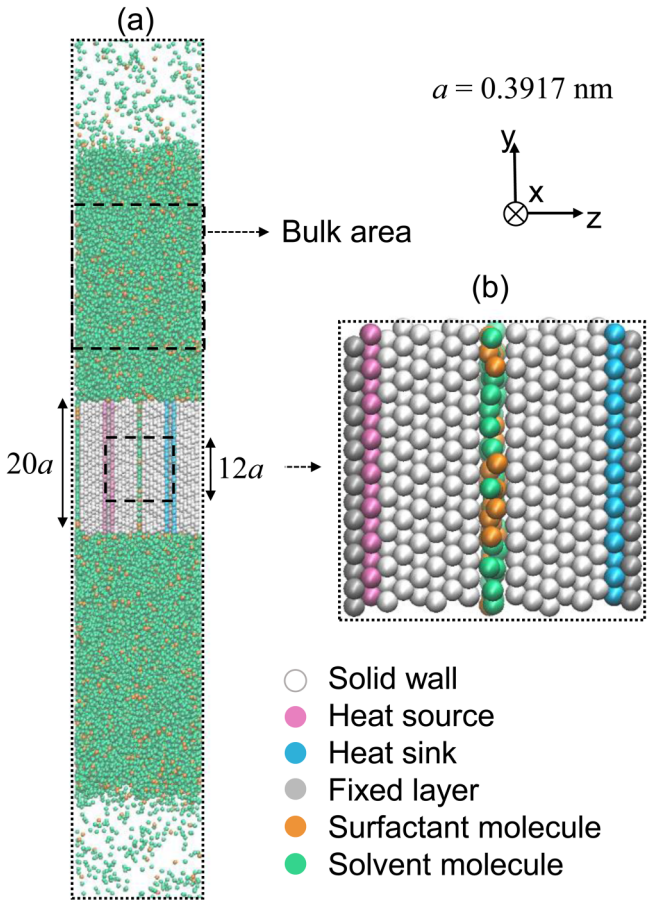

FIG. 1. Diagram of the simulation systems. In the large system (a), two solid walls were immersed into the liquid with different concentrations of surfactant, c_{surf}, in the bulk area, and the vapor area was sufficiently distant from the solid walls. The liquid composition of the small system (b) was obtained from the center area between solid walls of the large system (a), indicated by dashed lines. For large and small simulation systems, the surface separation of two solid walls, d_{ss}, was varied, and the heat flow from the heat source to the heat sink via the liquid film was induced.

walls with the same thickness were placed with the same surface separation in the z-direction, where the z-dimension of the system was varied from 7.46 nm to 11.54 nm. Each solid wall was constructed of 15 layers with the (111) FCC crystal plane normal to the z-direction with a layer spacing of 0.226 nm, and the two solid walls were positioned in a mirror-symmetric relation. The x-dimension of the solid wall was set to be the same as the system, and the y-dimension of the solid wall was set to $20a$, where $a = 0.3917$ nm is the lattice constant of platinum. The surface separation was measured by averaging the distance between the solid surface layers at the solid-liquid interfaces.

After an equilibrium MD simulation for 10 ns with a Nosé–Hoover thermostat at an average temperature of 120 K, the liquid molecules filled the gaps between the solid walls. Afterward, we expanded the system along the y direction symmetrical to 51.2 nm to produce an area for the vapor phase in order to maintain the pressure constant. We did not set the system to this size initially because there was a risk of gas pockets appearing at the solid surface.[23] Nonequilibrium molecular dynamics (NEMD) run for 20 ns was followed, where a Langevin thermostat with a damping coefficient of 100 fs was coupled to the solid layers of heat source and heat sink as shown in Fig. 1(b) with the control temperatures being set to 146 K and 93 K, respectively, in order to generate a heat flux along the z-direction from one solid wall to the other through the liquid film. Note that the averaging temperature of heat source and heat sink is not equal to 120 K, which was the control temperature during the equilibration run mentioned previously. This is because the heat sink settings were taken from our prior work,[11] which are an artifact of previous internal settings. Nonetheless, we have confirmed that the liquid temperature in the NEMD systems was approximately 120 K, which was due to a different thermal boundary resistance on each of the interfaces, and this small deviation in heat sink settings had a minuscule effect on the overall results. The y component of the total momentum of liquid molecules in all simulations in the first phase was zeroed by subtracting the center-of-mass velocity to keep the liquid distributed symmetrically in the y direction every 100 steps.

We constructed a number of systems by starting from different initial surface separations of two solid walls, d_{ss}, varying from 1.7σ to 13.2σ. We started from 1.7σ because at lower surface separation such as 1.4σ, the liquid could not fill the gap between solid walls. The final solid surface distances slightly changed due to a small expansion/contraction of the Pt crystal after the systems were equilibrated, which is shown in Table II. Because the change was small for all conditions, we used the initial surface separation distances when referring to these systems.

Furthermore, three systems of different surfactant concentrations, corresponding to different intercalation states, were generated for each surface separation by replacing some solvent molecules selected randomly with surfactant molecules after a 10 ns run of NEMD. Here, we define the bulk concentration of surfactant, c_{surf}, as that in the bulk area, as shown in Fig. 1(a), which was away by 1.5 nm from both the solid and vapor areas in the y direction in order to avoid the influence of the phase interface. The number of surfactant molecules was chosen so that the three cases would approximately correspond to $c_{surf} = 0\%$, $c_{surf} = 8\%$, and $c_{surf} = 48\%$ as shown in Table II. The final bulk concentrations after equilibration slightly deviated from these values by about ±0.5%, owing to the different adsorption states of the surfactant to the solid surfaces for each system. We carried out additional simulations for sensitivity analysis and found that a 0.82% difference in c_{surf} resulted in a 5.8% deviation in heat flux, which is less than the maximum standard error of mean in heat flux in the present study, 7%. We, therefore, conclude that the above difference in the surfactant concentration is negligible.

B. Second phase

In the second phase, using our in-house MD simulation package, we reconstructed a small system where a liquid film is in between two solid walls as shown in Fig. 1(b). The solid crystal

TABLE II. Initial surface separation, d_{ss}, and the bulk concentration of the surfactant in the large system, c_{surf}, and average surface separations, D, at equilibrium, the area number density of surfactant molecules, N_{surf}^{gap}, and that of solvent molecules, N_{solv}^{gap}, where $\sigma = 3.4236$ Å is the radius parameter of the liquid-liquid interaction represented by the LJ potential.

	Case 1				Case 2				Case 3			
Initial d_{ss} (σ)	c_{surf} (%)	D (σ)	N_{surf}^{gap} (Å^{-2})	N_{soly}^{gap} (Å^{-2})	c_{surf} (%)	D (σ)	N_{surf}^{gap} (Å^{-2})	N_{soly}^{gap} (Å^{-2})	c_{surf} (%)	D (σ)	N_{surf}^{gap} (Å^{-2})	N_{soly}^{gap} (Å^{-2})
1.7	0	1.54	0	0.023	7.51	1.55	0.036	0.011	48.15	1.55	0.058	0.001
2.0	0	1.92	0	0.041	7.75	1.92	0.034	0.021	48.22	1.92	0.061	0.003
2.3	0	2.26	0	0.038	8.02	2.26	0.024	0.029	47.97	2.26	0.063	0.008
2.6	0	2.59	0	0.067	7.85	2.59	0.034	0.060	47.71	2.59	0.101	0.017
2.9	0	2.89	0	0.084	7.96	2.89	0.030	0.073	47.79	2.89	0.099	0.023
3.3	0	3.25	0	0.087	7.95	3.25	0.029	0.080	47.84	3.25	0.103	0.032
4.0	0	3.91	0	0.139	7.97	3.91	0.033	0.125	47.65	3.91	0.128	0.052
4.6	0	4.57	0	0.181	7.74	4.57	0.040	0.159	47.64	4.57	0.150	0.074
6.6	0	6.55	0	0.298	7.81	6.55	0.049	0.264	47.43	6.55	0.203	0.133
13.2	0	13.16	0	0.684	7.76	13.16	0.079	0.618	47.61	13.16	0.385	0.335

plane and the surface separations of each system were set to be the same with those in the first phase after the equilibration. The liquid composition of each system was obtained from the central area of the liquid film in the first phase, illustrated by a dotted box in Fig. 1(a), with a length of $12a$ in the y direction. The dimension was chosen to avoid the effect of the solid-liquid interface normal to the y direction. The x and y dimensions of small systems were set to 3.86 nm with the periodic boundary conditions applied, and each solid wall consisted of 8 layers in the z-direction with 224 atoms per layer, where the outmost molecular layers of the two solid walls were fixed, and vacuum existed outside the walls. The area number density of surfactant molecules, N_{surf}^{gap}, and that of solvent molecules, N_{solv}^{gap}, in the liquid film are listed in Table II. Note that the composition in the liquid film in the small system [Fig. 1(b)] significantly differs from that in the bulk area [Fig. 1(a)], especially in the case of a system with a small gap, the surfactant molecules account for most of the liquid film. Additional MD runs using different initial molecular configurations have been carried out to estimate the standard deviation of the liquid film composition, which was found to be sufficiently small and to not affect our conclusion. (For example, for the case of smallest separation with $c_{surf} = 8\%$, the relative standard deviation in N_{surf}^{gap} and N_{solv}^{gap} were 1% and 4.4%, respectively.) The heat source layer and the heat sink layer shown in Fig. 1(b) were set at the same temperature with that in the first phase, i.e., 146 K and 93 K, respectively, by the Langevin thermostat with the same parameters as in the first phase. A NEMD simulation was conducted so that the same thermal condition as that in the first phase was imposed on the small systems, and the analysis data were obtained from a 10 ns production run after a 5 ns equilibration run.

III. RESULTS AND DISCUSSION

A. Density profile

Figure 2 shows density profiles for the system of $d_{ss} = 13.2\sigma$ with two surfactant concentrations. In this case, a bulk liquid state appears in the middle of the liquid region away from the solid surfaces, where no oscillatory behavior of density appears. These systems of $d_{ss} = 13.2\sigma$ are referred to as the bulk system hereafter. The density profiles of surface demonstrate that solid walls on both sides are composed of solid molecular layers. As the solid molecular layers become closer to the solid-liquid interface, the peak of

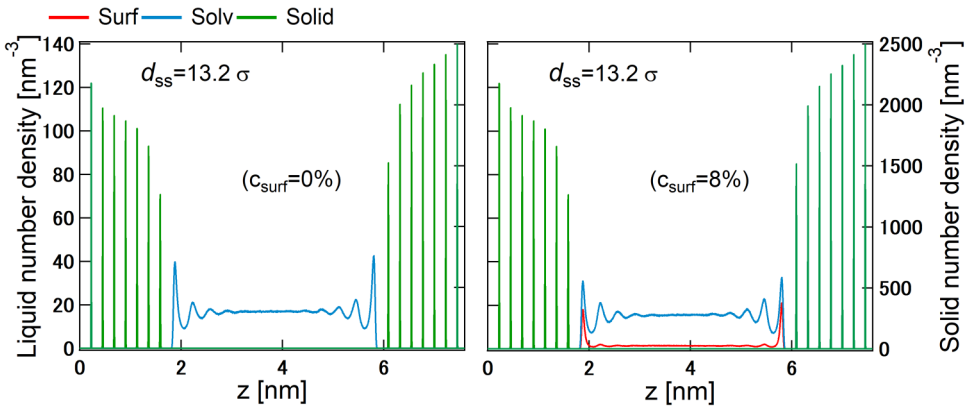

FIG. 2. Density profiles of the surfactant, solvent, and solid for the bulk system, $d_{ss} = 13.2\sigma$, for the cases of $c_{surf} = 0\%$ (left) and $c_{surf} = 8\%$ (right).

each layer becomes lower because the restraint between solid molecules becomes looser and the amplitude of molecular vibration increases. Density peaks of liquid molecules appear in the vicinity of the solid wall as a well-known liquid layer structure, where the surfactant is adsorbed on the solid surface. When the surface separation was equal or less than 4.6σ, the liquid film was composed of one to four molecular layers. Systems with 1–4 liquid layers are called N1, N2, N3, and N4, respectively.

The density distributions with $c_{surf} = 0\%$ for N1 and N2 are shown in Fig. 3 for several cases of the surface separation. For N1, the density peak of the solvent for $d_{ss} = 1.7\sigma$ [Fig. 3(a)] is about 2 times higher than that for $d_{ss} = 2.0\sigma$ [Fig. 3(b)], and the latter is near the highest density peak for the bulk system (left panel of Fig. 2). Three density profiles for N2 were obtained, where the highest peak of the solvent appears at $d_{ss} = 2.6\sigma$ [Fig. 3(d)], while the lowest one arises at $d_{ss} = 2.3\sigma$ [Fig. 3(e)], which is even lower than that for the bulk system.

The density profiles for the cases of $c_{surf} = 8\%$ are shown in Fig. 4. Comparing with Fig. 3, we found that the addition, i.e., intercalation, of surfactant molecules does not affect the number of adsorption layers, and the highest density peaks of the surfactant or solvent for N1 and N2 occur at the same distances of $d_{ss} = 1.7\sigma$ and $d_{ss} = 2.6\sigma$ as for systems without surfactant. The density peaks of solvent layers decrease with the addition of the surfactant because the adsorbed solvent molecules were replaced by the surfactant molecules, which have a stronger affinity with solid surfaces. Figure 4 shows that in the N1 state, the density peak of the surfactant layer is significantly higher than that of the solvent layer, whereas in the N2 state, the surfactant peaks become lower than the solvent peaks. This phenomenon that the surfactant in the solution tends to gather more in smaller gaps between solid walls has been observed for several types of surfactant solutions.[15,24,25]

B. Temperature distribution and thermal resistance

Typical temperature distribution profiles are shown in Fig. 5 for $d_{ss} = 1.7\sigma$ and $d_{ss} = 13.2\sigma$ with $c_{surf} = 8\%$. A significant temperature jump ΔT_w between the two solid walls was observed. The temperature jump can be decomposed: $\Delta T_w = \Delta T_H + \Delta T_{liquid} + \Delta T_C$, where ΔT_H and ΔT_C are the temperature jumps at the hot and cold solid-liquid interfaces, and ΔT_{liquid} is the temperature drop across the liquid film. The position of the solid-liquid interface was set as the midpoint between the density peak position of the solid surface layer and the density peak position of the liquid adsorption layer at the solid-liquid interface. All of these components were obtained from the temperature profile using an extrapolation method as applied in our previous works.[11,13] The interface temperature of the solid wall was obtained via linear extrapolation to the solid-liquid

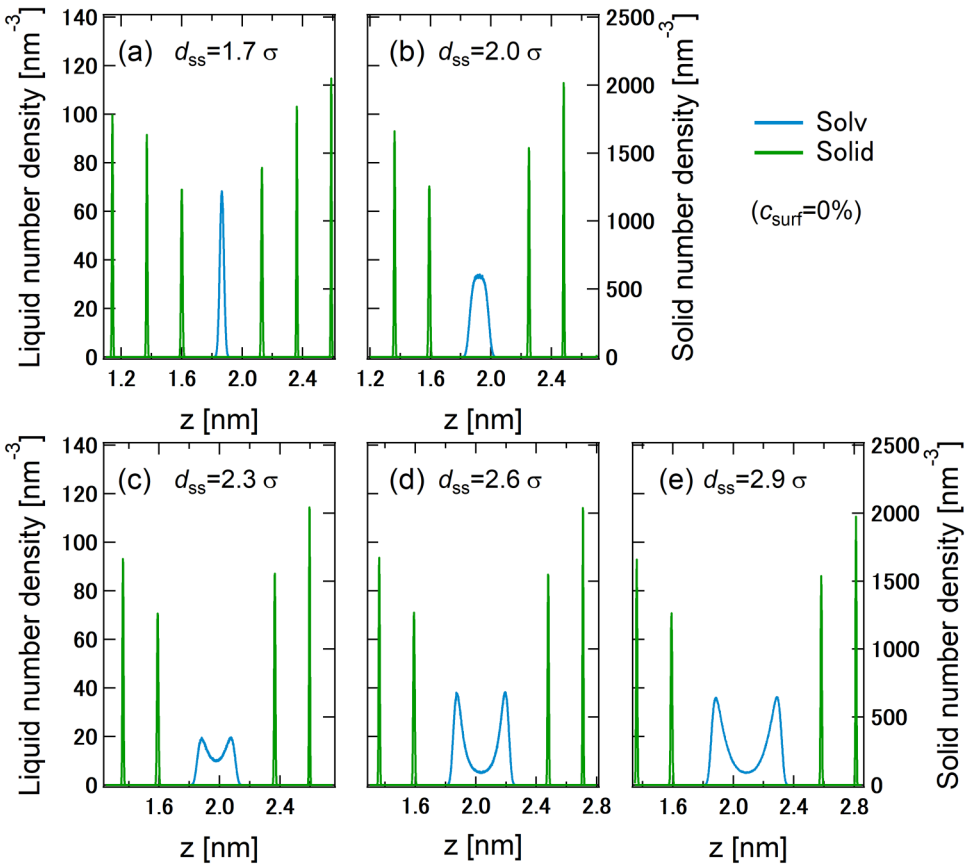

FIG. 3. Density profiles of the solvent and solid for a single-layer state (N1): (a) $d_{ss} = 1.7\sigma$ and (b) $d_{ss} = 2.0\sigma$ and a two-layer state (N2): (d) $d_{ss} = 2.3\sigma$, (e) $d_{ss} = 2.6\sigma$, and (f) $d_{ss} = 2.9\sigma$, where $c_{surf} = 0\%$.

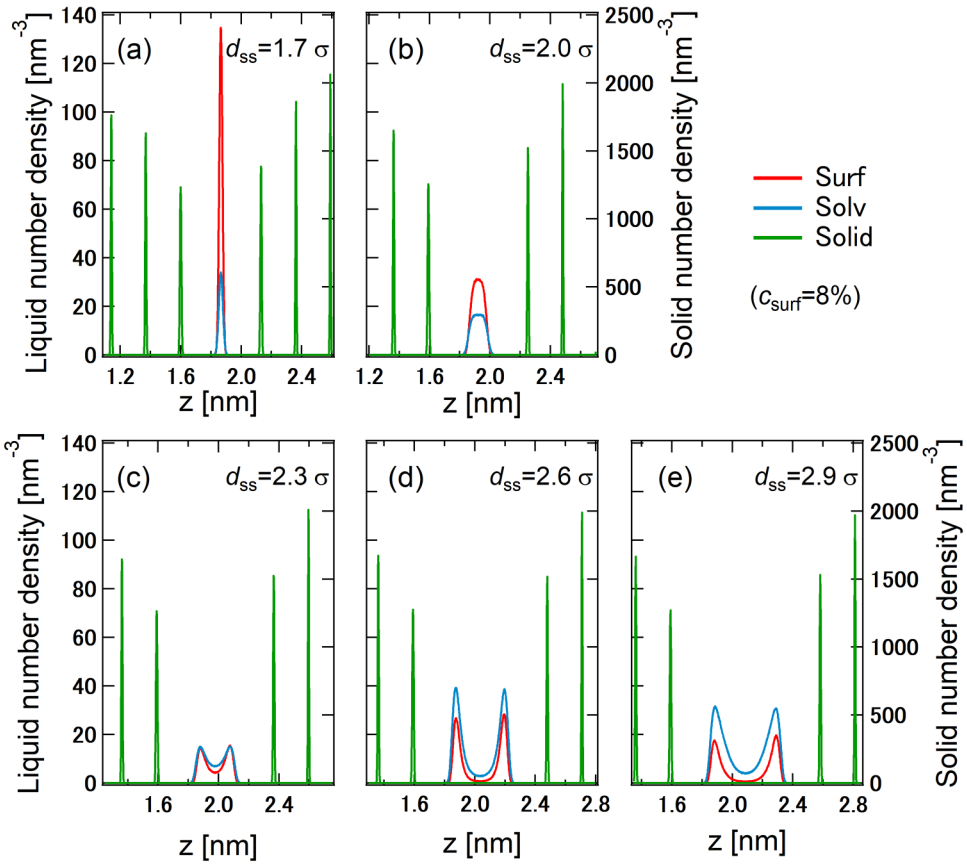

FIG. 4. Density profiles of the solvent, surfactant, and solid for a single-layer state (N1): (a) $d_{ss} = 1.7\sigma$ and (b) $d_{ss} = 2.0\sigma$ and a two-layer state (N2): (d) $d_{ss} = 2.3\sigma$, (e) $d_{ss} = 2.6\sigma$, and (f) $d_{ss} = 2.9\sigma$, where $c_{surf} = 8\%$.

interface, where all data points, except for the fixed layer, heat source/sink layer, and surface layer as shown in Fig. 1, were used. The interface temperature of liquid was set as the temperature of the adsorbed liquid layer at the solid-liquid interface for N1-N3 and the linear extrapolation of liquid temperature to the solid-liquid interface for N4 and larger, where all data except the first adsorption layer were used. The solid-liquid temperature jump was obtained as the difference between the interface temperatures of

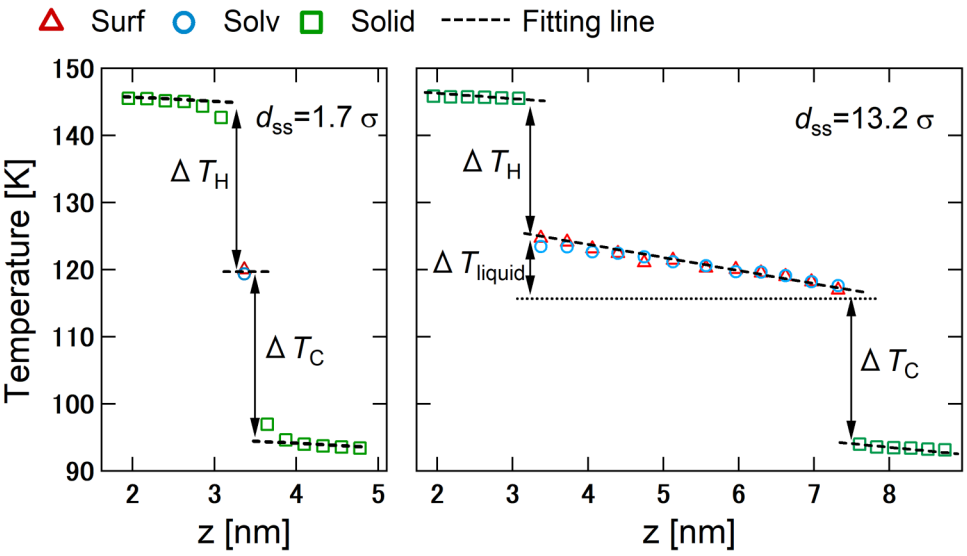

FIG. 5. Temperature distributions of the surfactant, solvent, and solid for $d_{ss} = 1.7\sigma$ (left) and $d_{ss} = 13.2\sigma$ (right) for the case of $c_{surf} = 8\%$. The temperature jump between the two solid walls ΔT_w is decomposed into solid-liquid temperature jumps at the hot and cold interfaces ΔT_H and ΔT_C and the temperature drop in the liquid film, ΔT_{liquid}.

solid and liquid, and the temperature drop was the temperature difference in the liquid film. The large temperature jump at the solid-liquid interface resulting from the significant interfacial thermal resistance was observed in Fig. 5. The temperature drop decreases linearly from the hot side to cold side in terms of the macroscopic heat conduction concept and is zero for the N1 states (left panel of Fig. 5) because temperature gradient could not be specified from the liquid film.

Overall thermal resistance R_{overall} is evaluated by

$$R_{\text{overall}} = \frac{-\Delta T_{\text{w}}}{J_z}. \tag{3}$$

The average of heat flux J_z through a control surface S_{xy} and over a control volume V in the z-direction were calculated by Eqs. (4) and (5), respectively,[26]

$$J_z S_{xy} = \sum_i \left[\left[\left(\frac{1}{2} m_i v_i^2 + \phi_i \right) / \Delta t \right] \frac{v_{i,z}}{|v_{i,z}|} + \frac{1}{2} \sum_i \sum_{j>i} [\mathbf{F}_{ij} \cdot (\mathbf{v}_i + \mathbf{v}_j)] \frac{z_{ij}}{|z_{ij}|} \right], \tag{4}$$

$$J_z V = \sum_i \left(\frac{1}{2} m_i v_i^2 + \phi_i \right) v_{i,z} v + \frac{1}{2} \sum_i \sum_{j>i} \left[\mathbf{F}_{ij} \cdot (\mathbf{v}_i + \mathbf{v}_j) z_{ij}^* \right]. \tag{5}$$

Here, m_i, v_i, and ϕ_i are the mass, velocity, and potential energy of the ith molecule; $\Delta t = 1$ fs, and the first term on the right side of Eq. (4) represents the transport energy in the z-direction carried by molecules across the control surface per time Δt; $z_{ij} = z_i - z_j$, $\mathbf{v}_i$ is the velocity vector of molecule i, and $\mathbf{F}_{ij}$ is the force that molecule j exerts on i, and the second term of Eq. (4) denotes the interaction energy across the control surface between molecules. Equation (5) represents the averaged heat flux in the z-direction over a control volume. The control surfaces were placed at the solid-liquid interface defined in the temperature distribution, and a control volume for the bulk system was placed at $3.5 < z < 5.5$ nm. The overall thermal resistance R_{overall} is expressed as

$$R_{\text{overall}} = R_{\text{H}} + R_{\text{C}} + R_{\text{liquid}}, \tag{6}$$

corresponding to the decomposition of ΔT_{w} mentioned above. Where R_{H} and R_{C} are the solid-liquid interfacial thermal resistances at the hot and cold interfaces, respectively, and R_{liquid} is the thermal resistance of the liquid. The decomposed thermal resistance according to Eq. (6) is shown in Fig. 6 only for the case of $c_{\text{surf}} = 8\%$, because other cases showed similar trends. Each profile has a form of oscillatory damping. The overall thermal resistances for the cases of $c_{\text{surf}} = 0\%$, $c_{\text{surf}} = 8\%$, and $c_{\text{surf}} = 48\%$ are shown in Fig. 7. When the number of layers is less than 4, the oscillation of overall thermal resistance occurs. The smallest surface separation case shows the smallest overall thermal resistance, which is similar to our previous work,[13] while other states show higher dependence on the surface separation than previous research.[13,14]

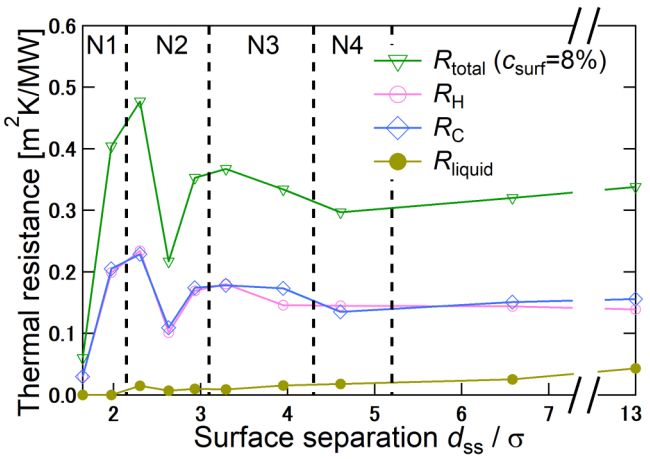

FIG. 6. Decomposed thermal resistance (the solid-liquid interfacial thermal resistances in the hot and cold interfaces, R_{H} and R_{C}, and thermal resistance of the liquid, R_{liquid}) as a function of surface separation for the case of $c_{\text{surf}} = 8\%$.

C. Adsorption phenomenon

1. Adsorption amount

In order to discuss the adsorption amount in relation to the molecular packing in the liquid film, we introduce an ideal surface separation for each N-layer state. If we consider that liquid molecules are horizontally (in the z-direction in our case) aligned so as to give the lowest potential energies, the surface separation d_{ideal} for this ideal state for each N-layer state is given as

$$d_{\text{ideal}} = 2r_{\text{S-L}} + (N-1)r_{\text{L-L}}, \tag{7}$$

where $r_{\text{S-L}}$ and $r_{\text{L-L}}$ are the distances of the potential minimum for the solid-liquid and liquid-liquid pair interactions, respectively.

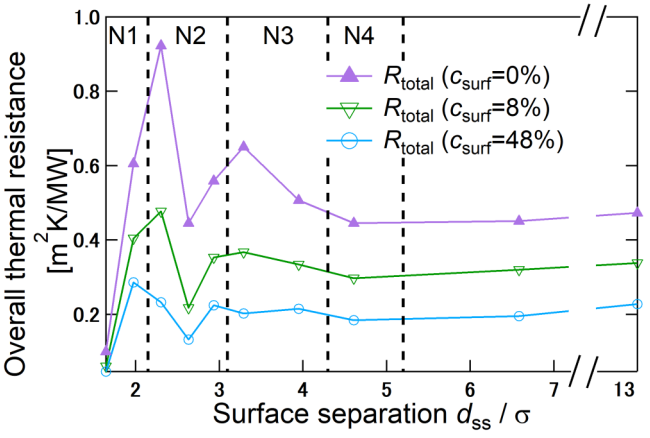

FIG. 7. Overall thermal resistance as a function of surface separation for the cases of $c_{\text{surf}} = 0\%$, $c_{\text{surf}} = 8\%$, and $c_{\text{surf}} = 48\%$.

TABLE III. Comparison of the surface separation d_{ss} in our system with the ideal surface separation d_{ideal} for each number of layers.

Number of layers	N1		N2			N3		N4
d_{ideal} (σ)	1.93		3.03			4.17		5.29
d_{ss} (σ)	1.7	2.0	2.3	2.6	2.9	3.3	4.0	4.6
d_{ss}/d_{ideal}	0.86	1.03	0.76	0.87	0.96	0.79	0.95	0.87

Table III gives the surface separations applied in the present study in relation to d_{ideal}.

The area number density of liquid molecules (the sum of the number of solvent and surfactant molecules) in the first adsorption layer is shown in Fig. 8 to quantify the adsorption amount. In each concentration, the "hot" and "cold" data points in the figure indicate the high and low temperature sides corresponding to the left and right solid walls, respectively, for N2-N4 systems. For N1 cases, there is only one layer between the solid walls and the "hot" or "cold" label is not meaningful; the data are plotted on the trend line of the "cold" side for convenience. All cases exhibit a similar oscillatory damping behavior, although their absolute values are different depending on the bulk concentration, c_{surf}. The oscillation has peaks at surface separations close to d_{ideal} for N1-N3 layer states. It could be interpreted that when the surface separation is close to d_{ideal}, the liquid molecules take the configuration with the lowest potential. Slightly more molecules are adsorbed onto the cold interface than onto the hot one, which is consistent with our previous study.[11]

2. Interface concentration of the surfactant

To investigate the aggregation of intercalating surfactant molecules in the gap between the solid surfaces, the interface concentrations

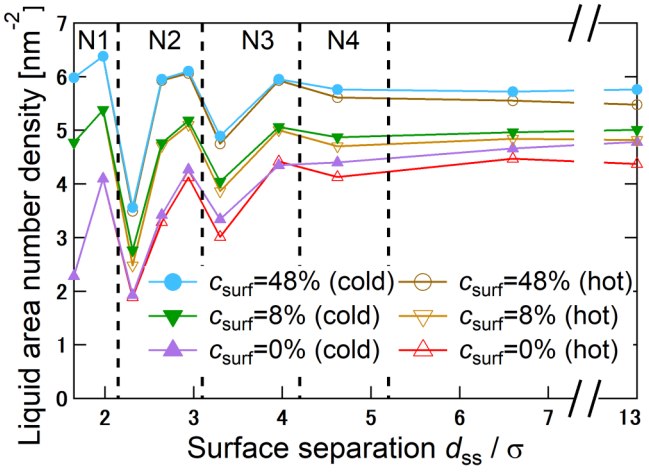

FIG. 8. Area number densities of liquid molecules (sum of the solvent and surfactant), in the first adsorption layer for the cases of c_{surf} = 0%, c_{surf} = 8%, and c_{surf} = 48%.

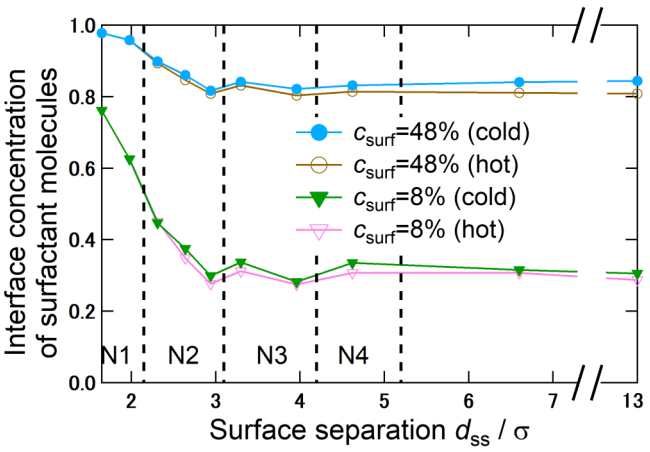

FIG. 9. Interface concentrations of the surfactant in the first adsorption layer for the cases of c_{surf} = 8% and c_{surf} = 48%, as a function of surface separation. The profiles for the sides of hot and cold walls are shown separately.

of the surfactant for the cases of c_{surf} = 8% and c_{surf} = 48% are shown in Fig. 9 as a function of surface separation. Because the absolute values of the number of adsorbed surfactant molecules oscillate with surface separation, the interface concentration of the surfactant is represented by the fraction of surfactant molecules to the total of the surfactant and solvent molecules in the first adsorption layer to show the results clearly. The profiles with different c_{surf} show similar tendencies although their absolute values are different. As the surface separation decreases, the interface concentration of the surfactant increases significantly, whereas the surface separations of more than N4 hardly affect the interface concentration of the surfactant.

3. Molecular packing affecting thermal resistance

After the surface separation exceeds N4, the amount of adsorbed surfactant molecules no longer depends on the surface separation, which can be observed from the density of adsorption layers in Fig. 8 and the interface concentration of the surfactant in Fig. 9. Due to this, the interfacial thermal resistance in Fig. 6 mostly converges to a single value at N4 and larger systems. On the other hand, the thermal resistance of the liquid gradually increases according to the manner of macroscopic heat conduction as thermal resistance is proportional to the liquid film thickness. For the range of surface separation displayed in Fig. 6, the contribution of the liquid film to the overall thermal resistance is negligibly small and the interfacial thermal resistance governs the overall thermal resistance. Compared with Fig. 7, the overall thermal resistance becomes lower with higher c_{surf} because higher c_{surf} results in the larger amount of adsorbed surfactant liquid molecules (Figs. 8 and 9) involved in heat transfer.

It should be noted that the state of the highest adsorption does not correspond to that of the highest peak in density distribution. For example, when one compares the two N1 states of $d_{ss} = 1.7\sigma$ and 2.0σ, the former state shows a higher peak in the density distribution in Fig. 3, but gives lower area number density

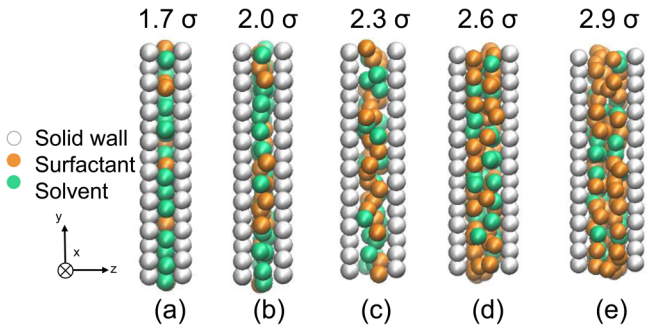

FIG. 10. Snapshots for different surface separation for the case of $c_{surf} = 8\%$. (a) and (b) correspond to a single-layer state (N1), whereas (c)–(e) correspond to a two-layer state (N2).

of liquid molecules in Fig. 8. Compared with Fig. 7, the minimum overall thermal resistance appears at $d_{ss} = 1.7\sigma$ for N1 and $d_{ss} = 2.6\sigma$ for N2. These distances correspond to the states of the highest density peaks for N1 and N2 (Figs. 3 and 4) rather than those of the highest area number density of the adsorption layer. This result is different from our previous works[11] where the thermal resistance depends on the area number density of the adsorption layer for systems with a relatively thick liquid film.

In order to understand the difference between the systems with the highest liquid layer density and the highest liquid density peaks, we took snapshots of systems after equilibrium for the case of $c_{surf} = 8\%$ as shown in Fig. 10. A significant change in the packing of liquid molecules is seen, even for the same number of adsorption layers. For N1, the molecular alignment for $d_{ss} = 1.7\sigma$, which gives the highest density peak, looks more ordered than that for $d_{ss} = 2.0\sigma$. The same is true for N2, where the surface separation of the highest density peak, $d_{ss} = 2.6\sigma$, has the most ordered two-layer structure. These results indicate that the state of molecular packing in the adsorption layers is more important as a factor influencing the thermal resistance of the ultrathin intercalation liquid film than the total amount of adsorbed molecules. In other words, when d_{ss} approaches an appropriate distance for liquid molecules to form a highly ordered structure, the solid-liquid interfacial thermal resistance is reduced significantly. In the present study, this separation was approximately given by $\sim 0.87 d_{ideal}$ in terms of the ideal surface separation d_{ideal} for N1 and N2 layer states as shown in Table III.

D. Analysis of VDOS

The analysis of molecular vibrational states has been applied to support the understanding of the heat-transfer mechanism at solid-liquid interfaces.[27,28] Here, the vibrational density of states (VDOS)[29] of surfactant molecules, solvent molecules, and solid molecules were calculated via the Fourier transformation of the velocity autocorrelation functions of x, y, and z velocity components. For the x and y components, no drastic difference was observed among cases with different surface separation d_{ss}. Therefore, only the z component for the cases of $c_{surf} = 8\%$ was plotted in Fig. 11, where the VDOS of liquid molecules in the adsorption layer and solid molecules in the surface layer are shown.

The nonzero value at zero frequency does not appear in N1, indicating the absence of self-diffusion in the z-direction. For all cases, the VDOS of surfactant molecules is closer to that of solid molecules than that of solvent molecules. Our previous research[11] showed that a heat path existed from the solid to solvent via the surfactant, and it can be interpreted that surfactant molecules have the role of mediating the heat transfer between solid and solvent molecules also in terms of VDOS.

For $d_{ss} = 1.7\sigma$ in Fig. 11(a), which has the highest ITC, the peak for the surfactant molecules appears at a rather higher frequency region than that in other cases, and a distinct overlap is found between the frequency bands of the surfactant and solid. Furthermore, the vibration frequency of the solvent is also closer to that of the solid, which is related to the fact that liquid molecules are more tightly constrained in the z-direction. This phononlike vibration is similar to our previous research[13] for single component liquids, while another one layer state for $d_{ss} = 2.0\sigma$ shows completely different VDOS. It is considered that this wide range overlapping due to the solidlike vibrational state of liquid molecules contributes to the significantly high ITC in $d_{ss} = 1.7\sigma$, while it is absent in all other cases.

E. Mechanism of interfacial thermal conductance (ITC) and solid-liquid affinity

The interfacial thermal conductance (ITC) is the inverse of interfacial thermal resistance and is given by the heat flux through the solid-liquid interface, $J_z^{interface}$, divided by the interfacial temperature jump. When evaluating $J_z^{interface}$ by Eq. (5), the first term is zero, as no molecules moved across the solid-liquid interface, i.e., the density at the interface was zero, because the solid surface was atomically flat, and thereby a depletion layer with no molecules was generated. With this in mind, $J_z^{interface}$ can be written as the sum of the intermolecular energy transfer (IET) between surfactant-solid, solvent-solid, and solid-solid molecules as follows:

$$J_z^{interface} = J_z^{surf\text{-}solid} + J_z^{solv\text{-}solid} + J_z^{solid\text{-}solid}. \tag{8}$$

By dividing each partial heat flux in the right-hand side of Eq. (8) by the temperature jump ΔT_H or ΔT_L for the hot and cold sides, respectively, the corresponding partial ITCs, $G_{surf\text{-}solid}$, $G_{solv\text{-}solid}$, and $G_{solid\text{-}solid}$, were calculated. The total ITC, G, with respect to a solid-liquid interface was obtained as the sum of these three components as

$$G = G_{surf\text{-}solid} + G_{solv\text{-}solid} + G_{solid\text{-}solid}. \tag{9}$$

A similar decomposition analysis has been reported by the authors for solid-liquid systems with surfactant additives[11] and a bulk mixture of simple liquids.[30]

The partial ITCs for the case of $c_{surf} = 8\%$ and $c_{surf} = 48\%$ at the cold interface are shown in Fig. 12 as a function of surface separation, while results for the hot interface are not shown due to their similarity. For the case of $c_{surf} = 8\%$, the surfactant-solid and

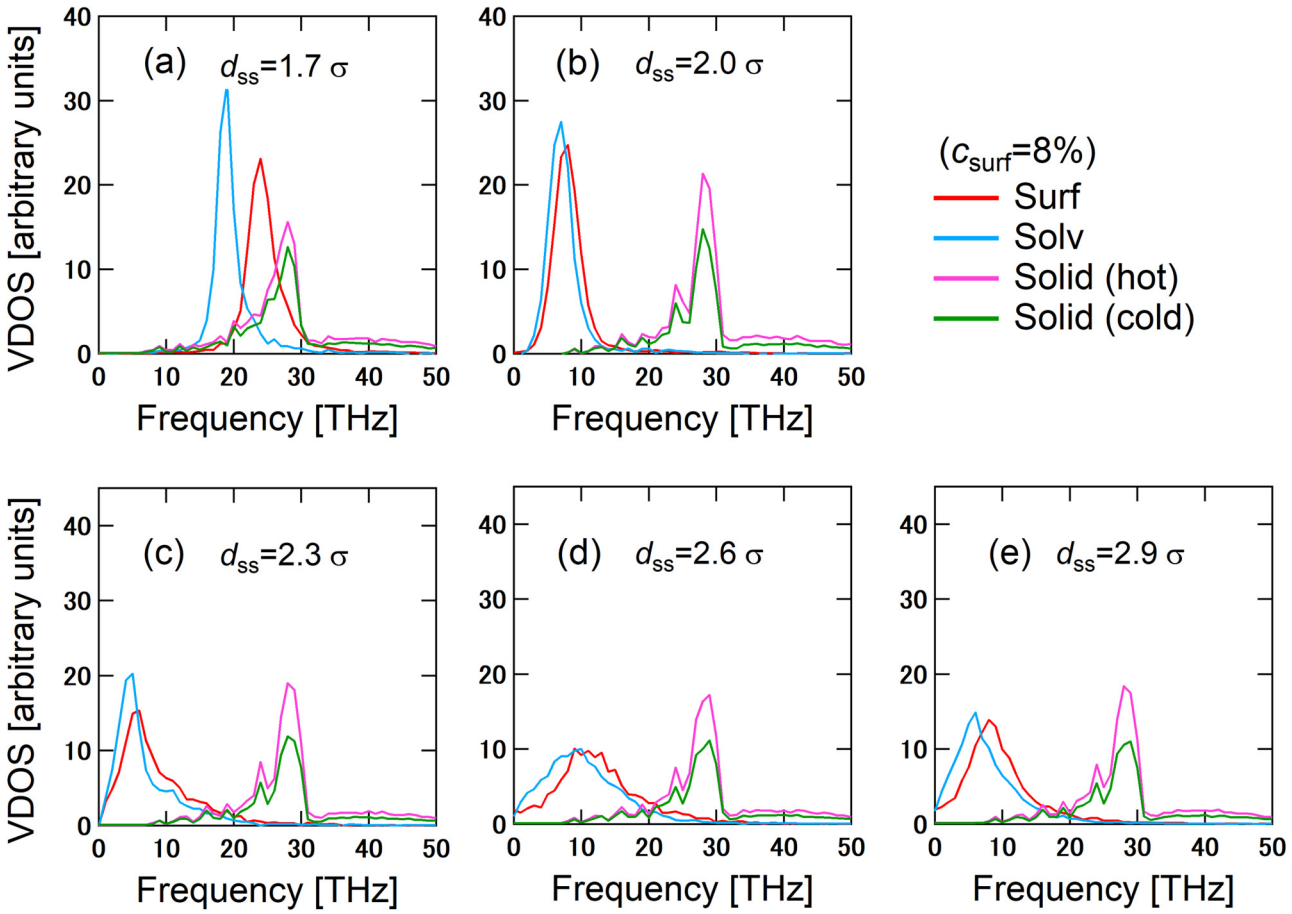

FIG. 11. VDOS in the direction of heat conduction (z component) of the solid molecules for the two solid layers directly in contact with the liquid, and the surfactant and solvent molecules in the adsorption layers for the cases of c_{surf} = 8%. (a) and (b) correspond to the N1 state, whereas (c)–(e) correspond to the N2 state. For liquid layers, only the result of the hot side only is shown.

solvent-solid IETs have similar contributions to the total ITC for most cases of d_{ss} except for the single-layer state. In contrast, in the case of c_{surf} = 48%, the total ITC is mostly accounted for by the surfactant-solid IET. The solid-solid IET has a nonminuscule contribution only in the smallest d_{ss}, and the value is relatively small compared to $G_{surf\text{-}solid}$. This result is different from our previous research,[13] where the solid-solid IET contributed significantly to ITC for the single-layer state. This is because in the solid-liquid-solid systems with a single liquid layer in our previous publication,[13] the surface separation was very small at about 0.6σ.

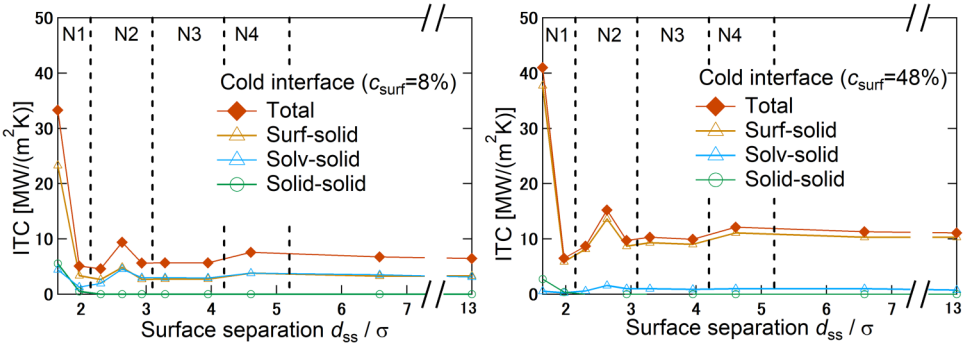

FIG. 12. Contributions of the surfactant-solid, solvent-solid, and solid-solid intermolecular energy transfer to the total interfacial thermal conductance (ITC), $G_{surf\text{-}solid}$, $G_{solv\text{-}solid}$, and $G_{solid\text{-}solid}$ for the cases of c_{surf} = 8% (left) and c_{surf} = 48% (right).

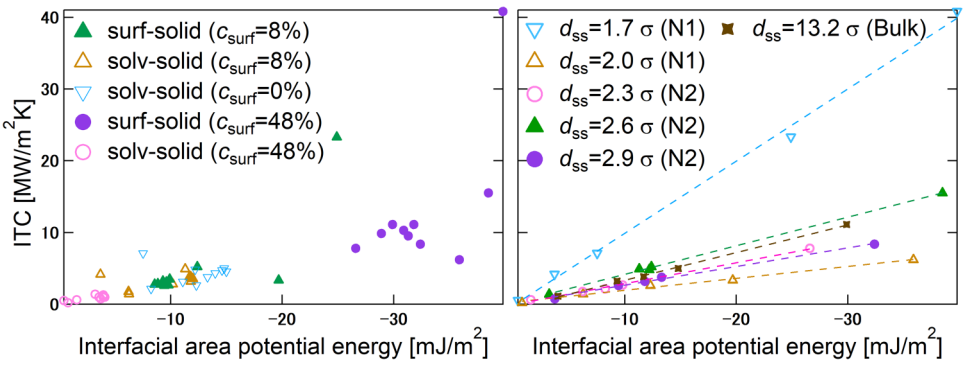

FIG. 13. Partial ITCs of surfactant-solid, $G_{surf\text{-}solid}$ and solvent-solid, $G_{solv\text{-}solid}$ as a function of their potential energy with the solid for the cases of c_{surf} = 0%, c_{surf} = 8%, and c_{surf} = 48%. The left panel values are grouped according to the partial ITC type and c_{surf}. The right panel shows the same results grouped by surface separation d_{ss}, for N1 states, N2 states, and the bulk system, while the linear fits for each d_{ss} are shown as the dashed line.

On the other hand, in the present study, the gap between solid walls had to be larger to allow the solvent and surfactant molecule to diffuse from the bulk area, and even a smaller surface separation of $d_{ss} = 1.4\sigma$ was too tight to allow liquid molecules into the gap. Thus, the molecular interactions between two solid walls are weaker due to larger surface separation.

The increase of ITC with increasing solid-liquid affinity has been observed in many past works,[31,32] including the authors' previous work about partial ITC of surfactant additives.[11] To investigate this relationship in the present system, $G_{surf\text{-}solid}$ and $G_{solv\text{-}solid}$ are plotted in Fig. 13 as a function of the solid-surfactant and solid-solvent intermolecular potential energy per unit area, respectively. The solid-surfactant and solid-solvent interfacial potential energies were obtained by summing all the interaction potential between corresponding solid-liquid molecular pairs, respectively. The left and right panels show the same values with different classifications to express the results more clearly. In the left panel of Fig. 13 where the results are classified by interaction type and c_{surf}, there is no distinct tendency.

A linear relation is found between the partial ITC and the potential energy independently of interaction type when grouped according to the surface separation as shown in the right panel of Fig. 13, where only the results for N1, N2, and the bulk system are shown because the remaining results were close to that of the bulk system. The gradient for $d_{ss} = 1.7\sigma$ is the highest and $d_{ss} = 2.6\sigma$ is the second highest. They correspond to the highest density peak (Figs. 3 and 4) for N1 and N2, and these are the only cases that have better interfacial heat transfer than the bulk system.

It is reasonable to consider that $G_{surf\text{-}solid}$ and $G_{solv\text{-}solid}$ are determined by the amount of surfactant-solid interacting pairs and solvent-solid interacting pairs and by the average contribution per single surfactant-solid and solvent-solid interaction. We obtained the latter quantity, $g_{surf\text{-}solid}$ and $g^{pair}_{solv\text{-}solid}$, for the per surfactant-solid and solvent-solid interaction, respectively, by dividing the partial ITC by the number of corresponding interacting molecular pairs as follows:

$$g^{pair}_{surf\text{-}solid} = \frac{G_{surf\text{-}solid}}{N^{gap}_{surf} \times N^{gap}_{solid}}, \tag{10}$$

$$g^{pair}_{solv\text{-}solid} = \frac{G_{solv\text{-}solid}}{N^{gap}_{surf} \times N^{gap}_{solid}}, \tag{11}$$

where N^{gap}_{surf} and N^{gap}_{solv} are the area number density of surfactant and solvent molecules in the first adsorption layer listed in Table II, and N^{gap}_{solid} is that of the solid molecules in the first surface layer. These values for the cold interface were plotted in Fig. 14.

When the number of layers was more than 4, $g^{pair}_{surf\text{-}solid}$ and $g^{pair}_{solv\text{-}solid}$ remain almost constant and independent of the concentration. Moreover, $g^{pair}_{surf\text{-}solid}$ is 2 times higher than $g^{pair}_{solv\text{-}solid}$. This is in accordance with the fact that the intermolecular potential for the surfactant-solid interaction was set to be 2 times stronger than that for the solvent-solid interaction as described in Sec. II. Thus, $g^{pair}_{surf\text{-}solid}$ and $g^{pair}_{solv\text{-}solid}$ are proportional to their intermolecular potential with the solid molecules, as was discussed in our previous research[11] for systems with an isolated solid-liquid interface.

As the surface separation decreases, $g^{pair}_{surf\text{-}solid}$ and $g^{pair}_{solv\text{-}solid}$ do not remain constant but vary considerably and become slightly higher with higher c_{surf}. It is considered that a higher c_{surf} improves the heat-transfer capability of both surfactant and solvent molecules. The peaks of $g^{pair}_{surf\text{-}solid}$ and $g^{pair}_{solv\text{-}solid}$ appear in the highest liquid density peak for N1 and N2, which means that each molecule can transfer

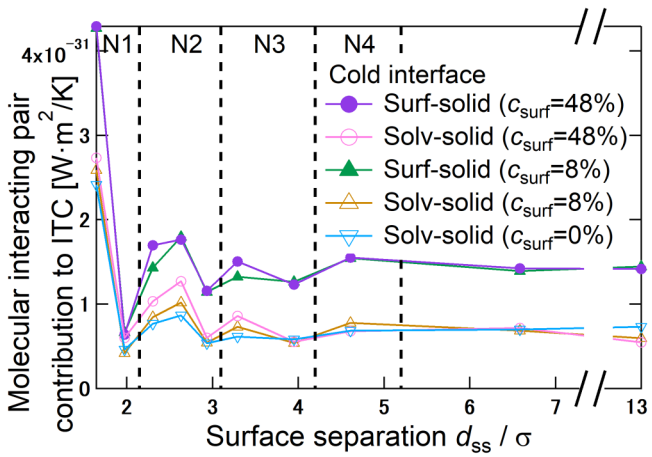

FIG. 14. Contributions to the total ITC from a single surfactant-solid interacting pair, $g^{pair}_{surf\text{-}solid}$, and solvent-solid interacting pair, $g^{pair}_{solv\text{-}solid}$, as a function of surface separation for the cases of c_{surf} = 0%, c_{surf} = 8%, and c_{surf} = 48%.

thermal energy most efficiently in a state of ordered molecular packing. This finding explains the more fundamental origin of the thermal resistance minimum discussed in Sec. III B.

IV. CONCLUSION

In this study, extending our previous research works about heat conduction across an ultrathin liquid film between closely positioned solid surfaces[13] and effects of surfactant additives on solid-liquid ITC,[11] we presented molecular dynamics simulations of an ultrathin film of the surfactant solution between contacting solid surfaces. The heat conduction across the two confining surfaces was analyzed for a variety of surface separations and surfactant concentration conditions in order to discover the key factor of contact thermal resistance reduction by the intercalation of the surfactant solution.

The overall thermal resistance between the solid surfaces confining the ultrathin liquid film was mostly accounted for by the solid-liquid interfacial thermal resistance. The interfacial thermal resistance of a given system was characterized by various measures including the interface concentration of the surfactant that would correspond to the intercalation state, molecular packing, VDOS profile, decomposition of ITC, and solid-liquid potential energy.

The higher the surfactant concentration, c_{surf}, the lower the interfacial thermal resistance observed for all the cases with different surface separation, because surfactant molecules were more efficient heat carriers than solvent molecules in the context of solid-liquid heat transport. This result indicated that the additive of the surfactant is an effective method to decrease the intersolid thermal resistance not only for a relatively thick liquid film shown in our previous work[11] but also for cases with small surface separation.

When the number of adsorbed liquid layers was less than 4, as the surface separation decreased, the interface concentration of the surfactant increased, while the interfacial thermal resistance damply oscillated. The smallest surface separation case showed the lowest interfacial thermal resistance, which was due to the fact that the average contributions to ITC per surfactant-solid interacting pair and solvent-solid interacting pair were maximized. VDOS showed a wide overlap of vibrational states between solid and surfactant molecules for the smallest surface separation case, while VDOS could not fully reflect the oscillating ITC in relation to surface separation for other cases. Surface separation was found to be a key factor determining the interfacial thermal resistance. Additionally, for a given surface separation distance, ITC was proportional to the well depth of solid-liquid potential energy.

The lowest interfacial thermal resistance occurred when the liquid film showed most ordered molecular packing at certain surface separation commeasurable to the size of solvent molecules, where the density peak of liquid molecules became the highest, rather than the highest area number density of liquid molecules in the adsorption layers. This was different from our previous research,[11] where the area number density of adsorbed liquid molecules was shown as the determining factor of the interfacial thermal resistance for a relatively thick liquid film. From the point of application of TIM in nanoelectronic devices, the surface separation between solid components is expected to vary, which according to our current results would create highly inhomogeneous ITC and temperature difference with thermal stress resulting from it.

ACKNOWLEDGMENTS

This work was supported by JST CREST Grant No. JPMJCR17I2, Japan. Numerical simulations were performed on the Supercomputer system "AFI-NITY" at the Advanced Fluid Information Research Center, Institute of Fluid Science, Tohoku University.

REFERENCES

[1]A. R. bin Saleman, H. K. Chilukoti, G. Kikugawa, M. Shibahara, and T. Ohara, Int. J. Heat Mass Transfer **105**, 168 (2017).
[2]R. Prasher, Proc. IEEE **94**, 1571 (2006).
[3]J. Xu and T. S. Fisher, Int. J. Heat Mass Transfer **49**, 1658 (2006).
[4]G. Kikugawa, T. Ohara, T. Kawaguchi, I. Kinefuchi, and Y. Matsumoto, Int. J. Heat Mass Transfer **78**, 630 (2014).
[5]P. J. O'Brien, S. Shenogin, J. Liu, P. K. Chow, D. Laurencin, P. H. Mutin, M. Yamaguchi, P. Keblinski, and G. Ramanath, Nat. Mater. **12**, 118 (2013).
[6]Y. Ma, G. Lu, C. Shao, and X. Li, Fuel **237**, 989 (2019).
[7]Z. Xuefen, L. Guiwu, W. Xiaoming, and Y. Hong, Appl. Surf. Sci. **255**, 6493 (2009).
[8]V. E. Nakoryakov, N. S. Bufetov, N. I. Grigorieva, and R. A. Dekhtyar, Int. J. Low-Carbon Technol. **1**, 273 (2006).
[9]M. A. Ahmadi and S. R. Shadizadeh, Energy Fuels **26**, 4655 (2012).
[10]X. Wu, Y. Ni, J. Zhu, N. D. Burrows, C. J. Murphy, T. Dumitrica, and X. Wang, ACS Appl. Mater. Interfaces **8**, 10581 (2016).
[11]Y. Guo, D. Surblys, Y. Kawagoe, H. Matsubara, X. Liu, and T. Ohara, Int. J. Heat Mass Transfer **135**, 115 (2019).
[12]Z. Liang and H.-L. Tsai, Phys. Rev. E **83**, 041602 (2011).
[13]X. Liu, D. Surblys, Y. Kawagoe, A. R. Bin Saleman, H. Matsubara, G. Kikugawa, and T. Ohara, "A molecular dynamics study of thermal boundary resistance over solid interfaces with an extremely thin liquid film," Int. J. Heat and Mass Transfer (published online).
[14]Z. Liang and H.-L. Tsai, Phys. Rev. E **83**, 061603 (2011).
[15]P. Angelikopoulos, S. Al Harthy, and H. Bock, J. Phys. Chem. B **113**, 13817 (2009).
[16]V. Subramanian and W. A. Ducker, Langmuir **16**, 4447 (2000).
[17]L. M. Grant and W. A. Ducker, J. Phys. Chem. B **101**, 5337 (1997).
[18]J. Park, J. Huang, W. Wang, C. J. Murphy, and D. G. Cahill, J. Phys. Chem. C **116**, 26335 (2012).
[19]E. Ruckenstein and H. Liu, Ind. Eng. Chem. Res. **36**, 3927 (1997).
[20]H. Ö. Pamuk and T. Halicioglu, Phys. Status Solidi A **37**, 695 (1976).
[21]P. Spijker, A. J. Markvoort, S. V. Nedea, and P. A. J. Hilbers, Phys. Rev. E **81**, 011203 (2010).
[22]S. Plimpton, J. Comput. Phys. **117**, 1 (1995).
[23]S. Maruyama and T. Kimura, Heat and Technology **18**, 69 (2000).
[24]R. Steitz, P. Müller-Buschbaum, S. Schemmel, R. Cubitt, and G. H. Findenegg, Europhys. Lett. **67**, 962 (2004).
[25]V. V. Yaminsky, B. W. Ninham, H. K. Christenson, and R. M. Pashley, Langmuir **12**, 1936 (1996).
[26]T. Ohara, J. Chem. Phys. **111**, 6492 (1999).
[27]H. A. Patel, S. Garde, and P. Keblinski, Nano Lett. **5**, 2225 (2005).
[28]G. Kikugawa, T. Ohara, T. Kawaguchi, E. Torigoe, Y. Hagiwara, and Y. Matsumoto, J. Chem. Phys. **130**, 074706 (2009).
[29]Z. Liang and M. Hu, J. Appl. Phys. **123**, 191101 (2018).
[30]Y. Fang, G. Kikugawa, H. Matsubara, T. Bessho, S. Yamashita, and T. Ohara, Fluid Phase Equilib. **429**, 293 (2016).
[31]C. U. Gonzalez-Valle, S. Kumar, and B. Ramos-Alvarado, ACS Appl. Mater. Interfaces **10**, 29179 (2018).
[32]D. Alexeev, J. Chen, J. H. Walther, K. P. Giapis, P. Angelikopoulos, and P. Koumoutsakos, Nano Lett. **15**, 5744 (2015).